B. Addendum to Chapter XI (Addendum B). Lift forces on a cylindrical particle in plane Poiseuille flow of shear thinning fluids

Wang and Joseph [2003] have extended the analyses of the slip velocities and the lift on particles in plane Poiseuille flow from Newtonian fluids to shear thinning fluids. Explicit formulas for the lift force have been derived in terms of the slip velocity and angular slip velocity by correlating the data from numerical experiments.

▪ *The lift force on a particle in a shear flow*

Different analytical expressions for the lift force on a particle in a shear flow can be found in the literature. Auton [1987] gave a formula for the lift on a particle in an inviscid fluid in which uniform motion is perturbed by a weak shear. Bretherton [1962] found an expression for the lift per unit length on a cylinder (two-dimensional sphere) in an unbounded linear shear flow at small values of Reynolds number. Saffman [1965, 1968] gave an expression for the lift on a sphere in an unbounded linear shear flow. Saffman's equation is in the form of the slip velocity multiplied by a factor, which can be identified as a density multiplied by a circulation as in the famous formula $\rho U\Gamma$ for aerodynamic lift. A number of formulas like Saffman's exist and a review of such formulas can be found in McLaughlin [1991]. Formulas like Saffman's cannot explain the experiments by Segrè and Silberberg [1961, 1962]. They studied the migration of dilute suspensions of neutrally buoyant spheres in pipe flows and found the particles migrate away from both the wall and the centerline and accumulate at a radial position of about 0.6 times the pipe radius. There is nothing in formulas like Saffman's to account for the migration reversal near 0.6 of the radius.

The effect of the curvature of the undisturbed velocity profile was found to be important to understand the Segrè and Silberberg effect. Ho and Leal [1974] analyzed the motion of a neutrally buoyant particle in both simple shear flows and plane Poiseuille flows. They found that for Couette flow, the equilibrium position is the centerline; whereas for Poiseuille flow, it is 0.6 of the channel half-width from the centerline, which is in good agreement with Segrè and Silberberg.

Choi and Joseph [2001], Patankar, Huang, Ko and Joseph [2001] and Joseph and Ocando [2002] studied particle lift in plane Poiseuille flows by direct numerical simulation. They showed that multiple equilibrium states exist for heavy particles in plane Poiseuille flows. These equilibrium states can be stable or unstable and the distinction leads to division of the channel into alternating stability regions in the following order: wall – stable – unstable – stable – unstable – centerline (see Fig. B.3).

Joseph and Ocando [2002] analyzed the role of the slip velocity and the angular slip velocity on migration and lift. They showed that the discrepancy Ω_s -Ω_{se}, where Ω_{se} is the angular slip velocity at equilibrium position, is the quantity that changes sign across the equilibrium position. Thus, this discrepancy can be used to account for the migration from both the wall and the centerline to the equilibrium position.

Power law correlations are frequently observed in studies of solid-liquid flows. A famous example is the Richardson-Zaki correlation, which is obtained by processing the data of fluidization experiments. The Richardson-Zaki correlation describes the

complicated dynamics of fluidization by drag and is widely used for modeling the drag force on particles in solid-liquid mixtures. Correlations can also be drawn from numerical data; for example, power law correlations for single particle lift and for the bed expansion of many particles in slurries were obtained by processing simulation data (Patankar *et al.* [2001]; Choi and Joseph [2001]; Patankar, Ko, Choi, and Joseph [2001]). The prediction of power laws from numerical data suggests that the same type correlations could be obtained from experimental data as was done by Patankar, Joseph, Wang, Barree, Conway and Asadi [2002] and Wang, Joseph, Patankar, Conway and Barree [2003]. The existence of such power laws is an expression of self-similarity, which has not yet been predicted from analysis or physics. The flow of dispersed matter appears to obey those self-similar rules to a large degree (Barenblatt [1996]).

Most of studies on migration and lift are for Newtonian fluids. However, in many of the applications the fluids used are not Newtonian and shear thinning is one of the most important non-Newtonian properties. Papers treating the migration of particles in shear flows of shear thinning fluids were done by Huang, Feng, Hu and Joseph [1997], Huang, Hu and Joseph [1998] and especially by Huang and Joseph [2000]. All these authors used the Carreau-Bird viscosity function (B.1) but only Huang and Joseph [2000] studied the case when there is shear thinning but no normal stresses.

In this addendum, we extend previous studies of lift on a cylindrical particle in plane Poiseuille flows of Newtonian fluids to shear thinning fluids. We show that the pattern of the stability regions in shear thinning fluids is the same as that in Newtonian fluids. The effects of shear thinning on the distribution of the stability regions are discussed. We verify that the angular slip velocity discrepancy changes sign across the equilibrium position for both neutrally buoyant particles and heavy particles. We derive power law correlations for the lift force in terms of the slip velocity and angular slip velocity discrepancy and demonstrate that these correlations can be made completely explicit.

▪ *Governing equations*

The 2D computational domain is shown in Fig. B.1. l and W are the length and width of the channel respectively, and d is the diameter of the particle. The simulation is performed with a periodic boundary condition in the x-direction. The solutions are essentially independent of the channel length l for sufficiently large l. The geometric parameters are $W/d = 12$, $l/d = 22$. The values of these parameters are taken from Patankar *at al.* [2001] where they justified that the solutions are essentially independent of the selected geometric parameters.

A constant pressure gradient $-\overline{p}$ is applied which gives rise to Poiseuille flow and the direction of the gravity force is perpendicular to the flow direction. In simulations in periodic domains the fluid pressure P is split as follows:

$$P = p + \rho_f \mathbf{g}\cdot\mathbf{x} - \overline{p}\mathbf{e}_\mathbf{x}\cdot\mathbf{x} \;\Rightarrow\; -\nabla P = -\nabla p - \rho_f \mathbf{g} + \overline{p}\mathbf{e}_\mathbf{x}$$

where $\mathbf{e}_\mathbf{x}$ is the unit vector in x-direction, $\mathbf{x}$ is the position vector of any point in the domain and $\mathbf{g}$ is the gravitational acceleration. p is periodic and solved in simulations.

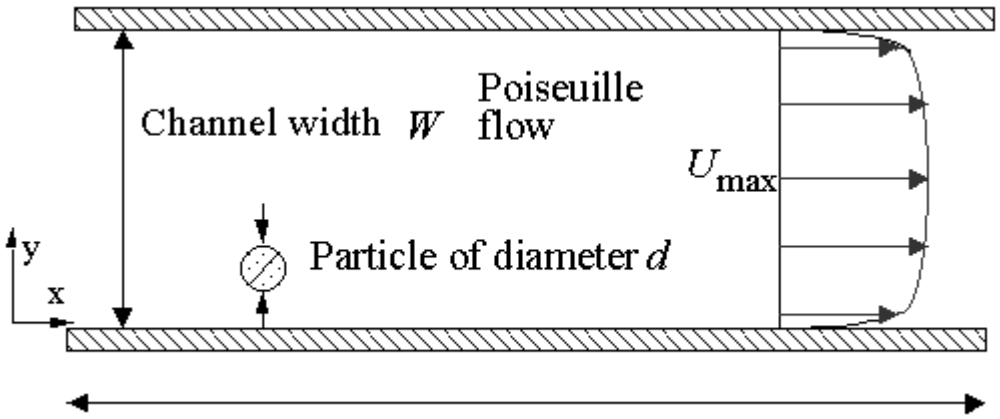

Figure B.1: The 2D rectangular computational domain.

We use the Carreau-Bird model for the shear thinning effects:

$$\frac{\eta-\eta_\infty}{\eta_0-\eta_\infty}=[1+(\lambda_3\dot{\gamma})^2]^{\frac{n-1}{2}} \tag{B.1}$$

where $\dot{\gamma}$ is the shear rate defined in terms of the second invariant of the rate of strain tensor **D**. The shear thinning index n is in the range of 0 – 1 and $\eta_0, \eta_\infty, \lambda_3$ are prescribed parameters. We use η_0=1.0 $g\cdot cm^{-1}\cdot s^{-1}$, η_∞/η_0=0.1 and λ_3=1.0s throughout our simulations.

We consider cylindrical particles of diameter d with the mass per unit length m = $\rho_p\pi d^2/4$ and the moment of inertia per unit length I = $\rho_p\pi d^4/32$. A dimensionless description of the governing equations can be constructed by introducing scales: the particle size d for length, V for velocity, d/V for time, V/d for angular velocity and $\eta_0 V/d$ for stress and pressure. We choose

$$V=\frac{\bar{p}W^2}{12\eta_0} \tag{B.2}$$

which is the average velocity of the undisturbed Poiseuille flow in Newtonian fluids. V can be related to the shear rate at the wall $\dot{\gamma}_w=\bar{p}W/(2\eta_0)$:

$$V=2\dot{\gamma}_w\frac{W}{12}=2\dot{\gamma}_w d\,.$$

Hat variables are dimensionless in the following part. The dimensionless governing equations are

$$\hat{\nabla}\cdot\hat{\mathbf{u}}=0\,,\quad R\left(\frac{\partial\hat{\mathbf{u}}}{\partial\hat{t}}+\left(\hat{\mathbf{u}}\cdot\hat{\nabla}\right)\hat{\mathbf{u}}\right)=-\hat{\nabla}\hat{p}+\frac{d}{W}\mathbf{e}_x+\hat{\nabla}\cdot\left[\Theta(\hat{\nabla}\hat{\mathbf{u}}+\hat{\nabla}\hat{\mathbf{u}}^T)\right] \tag{B.3}$$

for the velocity $\hat{\mathbf{u}}$ and pressure $\hat{p}$ of the fluid and

$$\frac{\rho_p}{\rho_f}R\frac{d\hat{\mathbf{U}}_\mathbf{p}}{d\hat{t}}=-G\mathbf{e}_y+\frac{d}{W}\mathbf{e}_x+\frac{4}{\pi}\oint\left\{-\hat{p}\mathbf{1}+\Theta(\hat{\nabla}\hat{\mathbf{u}}+\hat{\nabla}\hat{\mathbf{u}}^T)\right\}\cdot\mathbf{n}d\hat{\Gamma}\,, \tag{B.4}$$

$$\frac{\rho_p}{\rho_f} R \frac{d\hat{\boldsymbol{\Omega}}_{\mathbf{p}}}{d\hat{t}} = \frac{32}{\pi} \oint \left(\hat{\mathbf{x}} - \hat{\mathbf{X}}\right) \times \left(\left[-\hat{p}\mathbf{1} + \Theta(\hat{\nabla}\hat{\mathbf{u}} + \hat{\nabla}\hat{\mathbf{u}}^T) \right] \cdot \mathbf{n} \right) d\hat{\Gamma} \tag{B.5}$$

for the velocity $\hat{\mathbf{U}}_{\mathbf{p}}$ and angular velocity $\hat{\boldsymbol{\Omega}}_{\mathbf{p}}$ of the particle whose center of mass has the coordinate $\hat{\mathbf{X}}$. In equations (B.3) – (B.5) we use

$$R = \frac{\rho_f V d}{\eta_0}, G = \frac{(\rho_p - \rho_f) g d^2}{\eta_0 V} \text{ and } \Theta = \frac{\eta_\infty}{\eta_0} + (1 - \frac{\eta_\infty}{\eta_0}) \left[1 + (2\lambda_3 \dot{\gamma}_w)^2 \hat{\dot{\gamma}}^2 \right]^{\frac{n-1}{2}}.$$

The no-slip condition is imposed on the particle boundaries:

$$\hat{\mathbf{u}} = \hat{\mathbf{U}}_{\mathrm{p}} + \hat{\boldsymbol{\Omega}}_{\mathrm{p}} \times \left(\hat{\mathbf{x}} - \hat{\mathbf{X}}\right). \tag{B.6}$$

Following is a list of the dimensionless parameters:

ρ_p / ρ_f,	density ratio;
d/W,	aspect ratio;
η_∞ / η_0,	viscosity ratio;
$\Lambda^2 = (2\lambda_3 \dot{\gamma}_w)^2$,	shear rate parameter;
n,	shear thinning index;
$R = \frac{\rho_f V d}{\eta_0} = \frac{2\rho_f \dot{\gamma}_w d^2}{\eta_0} = \frac{\rho_f W d^2 \bar{p}}{\eta_0^2}$,	Reynolds number;
$G = \frac{(\rho_p - \rho_f) g d^2}{\eta_0 V} = \frac{d}{W} \frac{(\rho_p - \rho_f) g}{\bar{p}}$,	gravity parameter.

Instead of G, we use the gravity Reynolds number $R_G = R \cdot G = \frac{\rho_f (\rho_p - \rho_f) g d^3}{\eta_0^2}$.

W/d and η_∞ / η_0 are constant in our simulations; λ_3 is also constant, so Λ^2 would not provide more information. Thus ρ_p / ρ_f, R, n and R_G are the four dimensionless parameters at play. The Reynolds number R and shear thinning index n together, characterize an undisturbed Poiseuille flow. We define an average Reynolds number $\bar{R} = \rho_f u_0 d / \eta_0$ where u_0 is the average velocity of the undisturbed Poiseuille flow. In table B.1, we list the average Reynolds numbers $\bar{R}$ for flows characterized by (n, R) pairs. $\bar{R}$ increases significantly with n decreasing at a fixed R.

n	R	$\bar{R}$
1.0	20	20.00
0.9	20	24.28
0.8	20	30.48
0.7	20	39.70
1.0	40	40.00
0.9	40	51.84
0.8	40	69.97
0.7	40	97.89
1.0	80	80.00

0.9	80	110.72
0.8	80	160.06
0.7	80	237.60

Table B.1: Average Reynolds numbers $\overline{R}$ for flows characterized by (n, R) pairs.

- ***Undisturbed flow***

We refer to Poiseuille flow without particles as undisturbed flow. The dimensionless momentum equation in the x-direction for the undisturbed flow is

$$-\frac{d}{W} = \frac{d}{d\hat{y}}(\Theta \frac{d\hat{u}}{d\hat{y}}) . \tag{B.7}$$

An analytical solution for the Poiseuille flow of a Carreau-Bird fluid is not known. However, a numerical solution can be achieved by an iterative method. First $\hat{\dot{\gamma}}^0(\hat{y})$ is assumed to be the shear rate of the Poiseuille flow of a Newtonian fluid and $\Theta(\hat{\dot{\gamma}}^0(\hat{y}))$ is obtained. A new shear rate profile $\hat{\dot{\gamma}}^1(\hat{y})$ is then computed and the steps are repeated until $\hat{\dot{\gamma}}(\hat{y})$ converges. The velocity $\hat{u}(\hat{y})$ is obtained by integrating the shear rate.

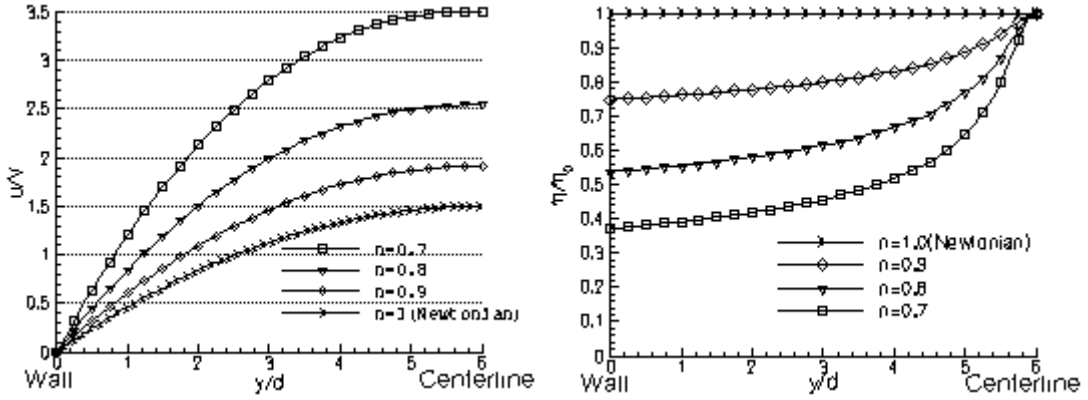

Figure B.2. The dimensionless velocity $u/V = u/(2\dot{\gamma}_w d)$ profiles (a) and the dimensionless viscosity η/η_0 profiles (b) of the Poiseuille flows with R = 40 and n = 0.7, 0.8, 0.9 and 1.0 (Newtonian fluid). Due to the symmetry of the profiles, only a half of the channel is plotted.

The velocity and viscosity profiles of the Poiseuille flows with R = 40 and n=0.7, 0.8, 0.9, and 1.0 (Newtonian fluid) are plotted in Fig. B.2. The velocity profiles are qualitatively similar to the parabolic profiles seen in flows of Newtonian fluids. At a fixed R, the maximum velocity in the channel increases significantly as n decreases. The viscosity profiles have their minimums at the wall (corresponding to the maximum $\dot{\gamma}$), and their maximums at the centerline (corresponding to zero $\dot{\gamma}$).

- ***Stable and unstable equilibrium regions***

An equilibrium is achieved for a freely moving and rotating cylindrical particle with a given density in a Poiseuille flow when the particle migrates to a position y_e of steady

rectilinear motion in which the acceleration and angular acceleration vanish and the hydrodynamic lift just balances the buoyant weight. Two types of simulations are performed, **unconstrained simulation** and **constrained simulation**. In unconstrained simulations, a particle is allowed to move and rotate freely to migrate to its equilibrium position. The initial translational and angular velocities of the particle are prescribed and initial-value problems are solved to obtain the equilibrium state. In constrained simulations, the position of the particle in the y-direction y_p is fixed and the particle is allowed to move in x-direction and rotate. The solution of the flow evolves dynamically to a steady state at which the lift force per unit length L on the particle is computed. Such a steady state will be an equilibrium at $y=y_p$ if the density of the particle is selected so that L just balances the buoyant weight per unit length, satisfying:

$$\hat{L} \overset{def}{=} \frac{L}{\rho_f g \pi d^2 / 4} = \frac{\rho_p}{\rho_f} - 1 \qquad \text{(B.8)}$$

where $\hat{L}$ is a dimensionless lift force and represents the ratio between the hydrodynamic lift force L and the buoyant force $\rho_f g \pi d^2/4$.

From the steady state values which evolve in constrained simulations, we are able to obtain $\hat{L}$ on the particle at any position y/d in the channel. We can divide the curve of $\hat{L}$ vs. y/d from the wall to the centerline into four branches by three "turning points" (see Fig. B.3). The "turning point" is defined as the position where the slope of the $\hat{L}$ vs. y/d curve is zero. On the first and third branches of steady solutions, the slope of $\hat{L}$ vs. y/d curve is negative, and the equilibrium points on these branches are stable. On the second and fourth branches of steady solutions, the slope of $\hat{L}$ vs. y/d curve is positive, and the equilibrium points are unstable. We will indicate the unstable branches by dotted lines in the figures.

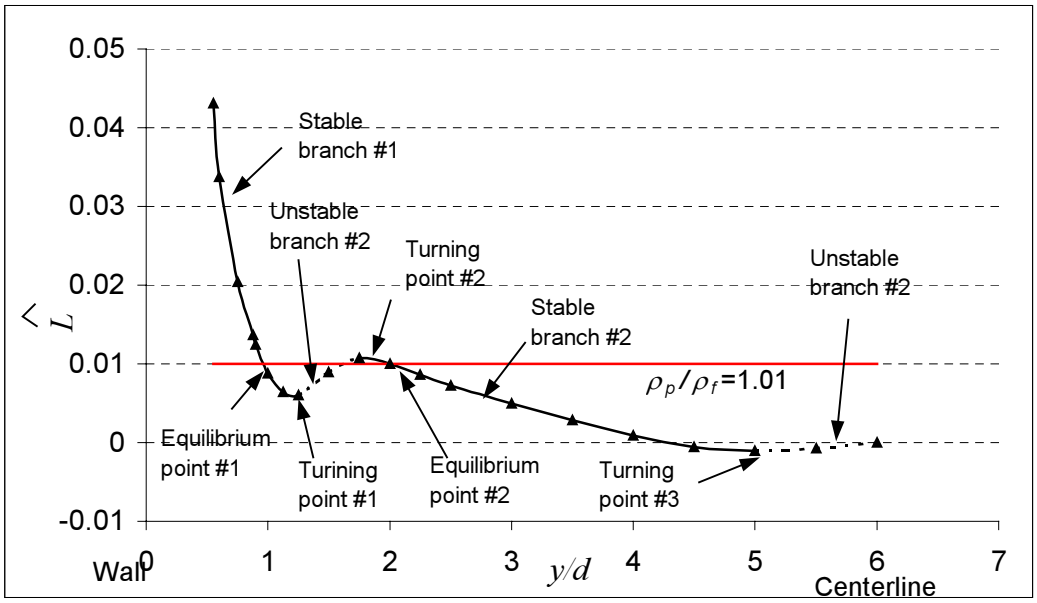

Figure B.3. A plot of $\hat{L}$ vs. y/d for a flow with n=0.8 and R = 20 from constrained simulations. The stable and unstable branches and three turning points are illustrated.

Unstable branches are indicated by dotted lines. Two stable equilibrium points for a particle with ρ_p/ρ_f *= 1.01 are shown.*

From the $\hat{L}$ vs. *y/d* curve, the equilibrium position for a particle with a certain ρ_p can be determined. The lift force required to balance the buoyant weight of a particle can be computed from (B.8). If we draw a line on which $\hat{L}$ equals to this required lift force, the points of intersections between this line and the $\hat{L}$ vs. *y/d* curve are the equilibrium points for this particle. For heavier-than-fluid particles with intermediate densities, there exist multiple stable equilibrium positions from the wall to the centerline (see Fig. B.3 where two stable equilibrium points for a particle with ρ_p/ρ_f = 1.01 are shown). However, for a neutrally buoyant particle ($\hat{L}$ = 0), only one stable equilibrium point exists from the wall to the centerline.

Ho and Leal [1974] studied the equilibrium position of a neutrally buoyant freely moving and rotating sphere between plane bounding walls. They assumed that the walls were so closely spaced that the lift could be obtained by perturbing Stokes flow with inertia. They calculated dimensionless lateral force vs. lateral position curves (equivalent to our $\hat{L}$ vs. *y/d* curve) for simple shear flow and 2D Poiseuille flow which are shown in Fig. B.4. Comparing the dashed line in Fig. B.4 which is for 2D Poiseuille flow and the $\hat{L}$ vs. *y/d* curve in Fig. B.3, one can see that both of the two plots imply the centerline is an unstable equilibrium position. However, the dashed line in Fig. B.4 indicates that there are two branches from the wall to the centerline: wall – stable – unstable – centerline, whereas four branches exist according to Fig. B.3. Ho and Leal only considered neutrally buoyant particle and did not include the gravity term in the governing equation used in their calculation. The frame of their work did not enable them to study the multi-equilibrium positions of heavier-than-fluid particles. The results shown in Figs. B.3 and B.4 are not strictly comparable; Ho and Leal studied spheres (3D) between plane walls at indefinitely small *R* whereas our calculation is for 2D particles at much higher Reynolds numbers.

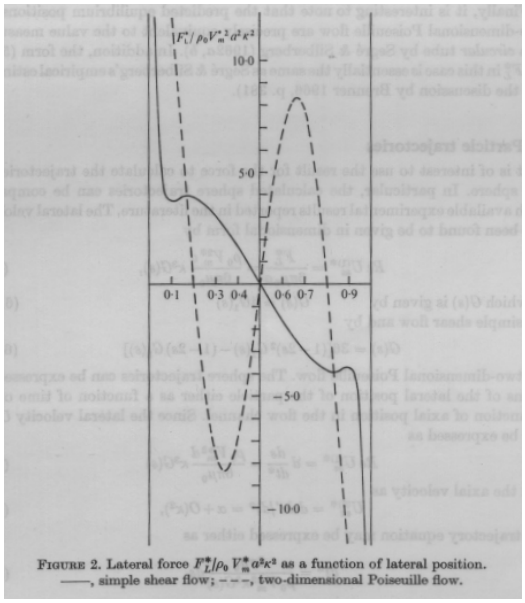

FIGURE 2. Lateral force $F_L^*/\rho_0 V_m^{*2} a^2 \kappa^2$ as a function of lateral position. ——, simple shear flow; – – –, two-dimensional Poiseuille flow.

Figure B.4. Lateral force as a function of lateral position, both in dimensionless form. —-, simple shear flow; - - -, 2D Poiseuille flow. (Adapted from Ho and Leal 1974)

The distribution of the equilibrium branches is affected by the shear thinning effects. The $\hat{L}$ vs. y/d curves are computed for the flows with R = 20, 40 and 80 and n=0.7, 0.8, 0.9 and 1.0 (Newtonian fluid). Two groups of typical curves are plotted in Figs. B.5 and B.6.

We find that when the shear thinning effects become stronger, the stable branch near the wall decreases in size; the unstable branch near the wall moves closer to the wall; the stable branch near the centerline increases in size; the unstable branch at the centerline decreases in size. The shrinkage of the unstable branch at the centerline implies that a particle could be lifted to a equilibrium position closer to the centerline if shear thinning effects are stronger. A closer equilibrium position to the centerline could also be achieved when pressure gradient is higher, as shown first in Patankar *et al.* [2001] and confirmed in our simulations. It seems that higher pressure gradient and stronger shear thinning both lead to stronger inertia effects and could lift a particle closer to the centerline. In the range of the Reynolds number and shear thinning index we simulated, the unstable branch at the centerline never vanishes. Patankar *et al.* [2001] reported that in 2D Poiseuille flows of an Oldroyd-B fluid at high Deborah number, the centerline can be a stable equilibrium position and the Segrè and Silberberg effect does not occur. We did not observe the same phenomenon in shear thinning fluids.

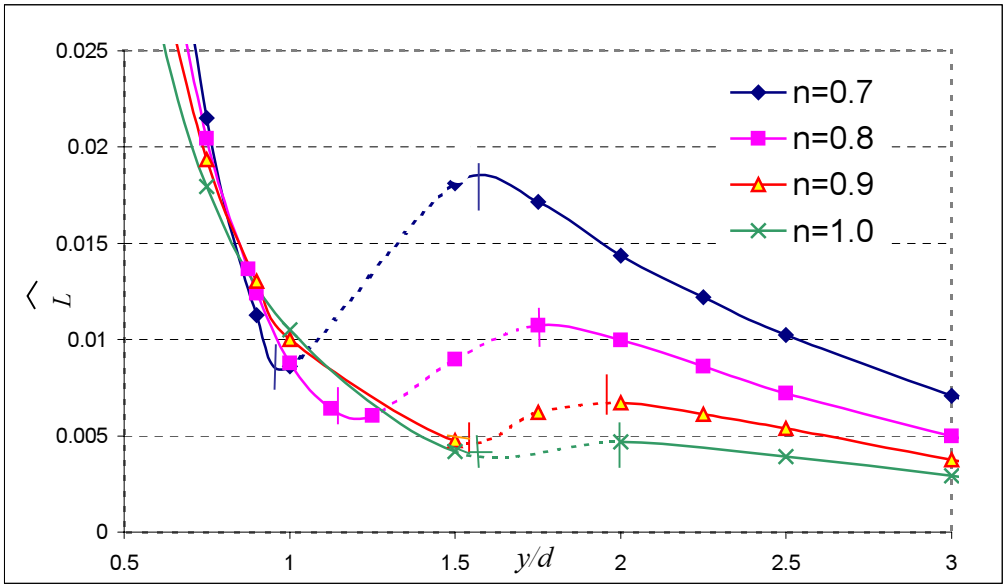

Figure B.5. Near-the-wall part of $\hat{L}$ vs. y/d curves of the Poiseuille flows with R = 20 and n=0.7, 0.8, 0.9 and 1.0 (Newtonian fluid). The unstable branches are indicated by dotted lines and their starting and ending points are marked by pairs of short vertical lines. With the shear index n decreasing, the stable branch near the wall decreases in size and the unstable branch near the wall moves closer to the wall.

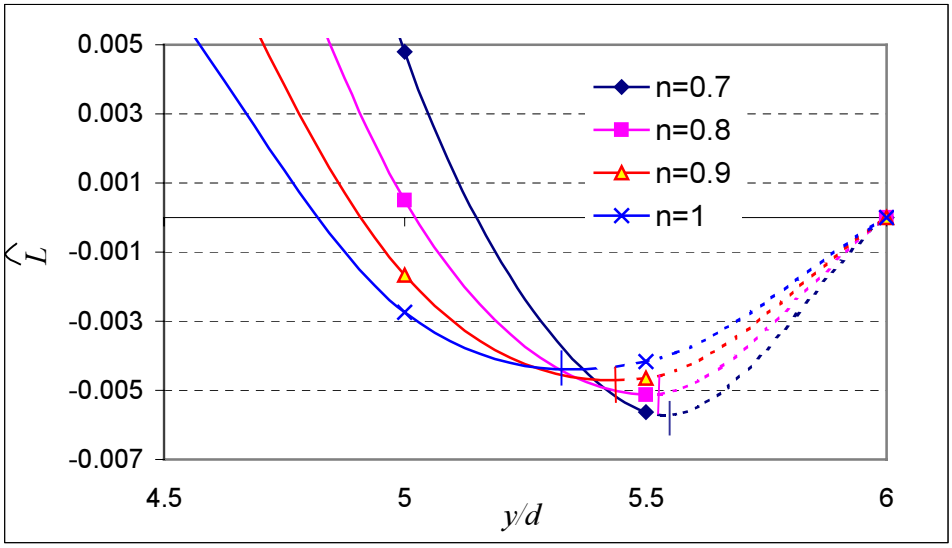

Figure B.6. Near-the-centerline part of $\hat{L}$ vs. y/d curves of the Poiseuille flows with R = 80 and n=0.7, 0.8, 0.9 and 1.0 (Newtonian fluid). The unstable branches are indicated by dotted lines and short vertical lines are used to mark the starting points of these unstable branches. With the shear index n decreasing, the unstable branch near the centerline decreases in size.

- ***Angular slip velocity discrepancy and net lift force***

Joseph and Ocando [2002] studied slip velocities and particle lift in 2D Poiseuille flows of Newtonian fluids. The slip velocity is U_s=U_f-U_p and the angular slip velocity is $\Omega_s = \Omega_p - \Omega_f$, where U_f and $\Omega_f = -\dot{\gamma}/2$ are the translational velocity and angular velocity of the undisturbed Poiseuille flow at the position of the particle and $\dot{\gamma}$ is the local shear rate. The net lift force is:

$$L_n = L - (\rho_p - \rho_f)\pi d^2 g/4 \;\Rightarrow\; \hat{L}_n = \hat{L} - (\frac{\rho_p}{\rho_f} - 1)\,. \qquad \text{(B.9)}$$

Joseph and Ocando found that the angular slip velocity discrepancy Ω_s -Ω_{se}, where Ω_{se} is the angular slip velocity at equilibrium, changes sign across the equilibrium position. Furthermore, they showed that across a stable equilibrium position, the net lift force L_n has the same sign as the discrepancy Ω_s -Ω_{se}; whereas across an unstable equilibrium position, the net lift force L_n has the opposite sign as the discrepancy Ω_s -Ω_{se}. In this section, we verify that these conclusions hold in shear thinning fluids using constrained simulations.

We fix a particle at positions slightly above ($y_p > y_e$) and below ($y_p < y_e$) its equilibrium positions and compute the steady state lift force and angular slip velocity Ω_s. For a neutrally buoyant particle, both stable and unstable equilibrium positions are investigated; for a heavy particle, both of its two stable equilibrium positions are investigated. Table B.2 shows the results for a neutrally buoyant particle and table B.3 shows those for a heavy particle.

y_e/d	4.35		6.0	
$\Omega_{se}/(2\dot{\gamma}_w)$	1.25×10^{-2}		0.0	
fixed y_p/d	4.33	4.36	5.95	6.05
$L/(\rho_f g\pi d^2/4)$	8.2×10^{-5}	-1.4×10^{-5}	-7.9×10^{-5}	7.7×10^{-5}
$(\Omega_s-\Omega_{se})/(2\dot{\gamma}_w)$	2.5×10^{-6}	-4.5×10^{-4}	5.8×10^{-5}	-5.3×10^{-5}

Table B.2. The steady state values of L and $\Omega_s-\Omega_{se}$ in dimensionless form at fixed positions slightly above ($y_p > y_e$) and below ($y_p < y_e$) the equilibrium positions of a neutrally buoyant particle in the flow with $n=0.7$ and $R=20$. The stable equilibrium position is $y_e/d=4.35$ with $\Omega_{se}/(2\dot{\gamma}_w)=1.25\times10^{-2}$. For the particle fixed below ($y_p/d = 4.33$), $\Omega_s-\Omega_{se}>0$ and $L>0$; for the particle fixed above ($y_p/d= 4.36$), $\Omega_s-\Omega_{se}<0$ and $L<0$. The unstable equilibrium position is the centerline with $y_e/d=6.0$ and $\Omega_{se}/(2\dot{\gamma}_w)=0$. For the particle fixed below ($y_p/d = 5.95$), $\Omega_s-\Omega_{se}>0$ but $L<0$; for the particle fixed above ($y_p/d=6.05$), $\Omega_s-\Omega_{se}<0$ but $L>0$.

y_e/d	0.918		2.26	
$\Omega_{se}/(2\dot{\gamma}_w)$	7.16×10^{-2}		4.95×10^{-2}	
fixed y_p/d	0.9	1.0	2.25	2.5
$L_n/(\rho_f g\pi d^2/4)$	1.88×10^{-3}	-6.4×10^{-3}	2.58×10^{-4}	-3.26×10^{-3}
$(\Omega_s-\Omega_{se})/(2\dot{\gamma}_w)$	4.88×10^{-4}	-1.44×10^{-3}	1.50×10^{-5}	-5.50×10^{-3}

Table B.3. The steady state values of the net lift force L_n and $\Omega_s-\Omega_{se}$ in dimensionless form at fixed positions above ($y_p > y_e$) and below ($y_p < y_e$) the equilibrium positions of a heavy particle ($\rho_p/\rho_f=1.024$) in the flow with $n=0.9$ and $R=40$. Two stable equilibrium positions exist: $y_e/d=0.918$ with $\Omega_{se}/(2\dot{\gamma}_w)=7.16\times10^{-2}$ and $y_e/d=2.26$ with $\Omega_{se}/(2\dot{\gamma}_w)=4.95\times10^{-2}$. For either one of the equilibrium positions, $\Omega_s-\Omega_{se}>0$ and $L_n>0$ when the particle is fixed below; $\Omega_s-\Omega_{se}<0$ and $L_n<0$ when the particle is fixed above.

Table B.2 and B.3 verify the conclusions about the discrepancy $\Omega_s-\Omega_{se}$, summarized as following: $\Omega_s-\Omega_{se}<0$ when $y_p > y_e$; $\Omega_s-\Omega_{se}>0$ when $y_p < y_e$. With a stable equilibrium as the reference state, negative $\Omega_s-\Omega_{se}$ leads to negative L_n, positive $\Omega_s-\Omega_{se}$ leads to positive L_n; with an unstable equilibrium position as the reference state, negative $\Omega_s-\Omega_{se}$ leads to positive L_n, positive $\Omega_s-\Omega_{se}$ leads to negative L_n. ($L_n=L$ in the case of a neutrally buoyant particle.) These conclusions are for the lift force and slip velocity in steady flows and do not hold generally for a free particle with accelerations.

- ***Lift correlations***

Motivated by the conclusion that $\Omega_s-\Omega_{se}$ has the same sign as L_n across a stable equilibrium position, we seek the correlations between L_n and the product $U_s(\Omega_s-\Omega_{se})$. Such correlations may be constructed by analogy with the classical lift formula $L=CU\Gamma$ of aerodynamics. The proper analogs of U and Γ in the present context are U_s and $\Omega_s-\Omega_{se}$ as first propsed in Joseph and Ocando [2002]. We proceed as follows to obtain the correlations. First we compute L, U_s and Ω_s as functions of y by constrained simulations in a steady flow with Reynolds number R and shear thinning index n. Then we correlate dimensionless parameters based on L and $U_s(\Omega_s-\Omega_{se})$ to power law formulas. These steps

are repeated for different flows identified by (R, n) pairs and lead to correlations for each flow. The coefficients in such correlations are functions of R and n which can be obtained by data fitting analyses. Finally we obtain correlations between dimensionless L and $U_s(\Omega_s - \Omega_{se})$ with coefficients expressed as functions of R and n.

Figure B.7 shows the relative values of L, U_s and Ω_s in the steady flow with R= 20 and n=0.9.

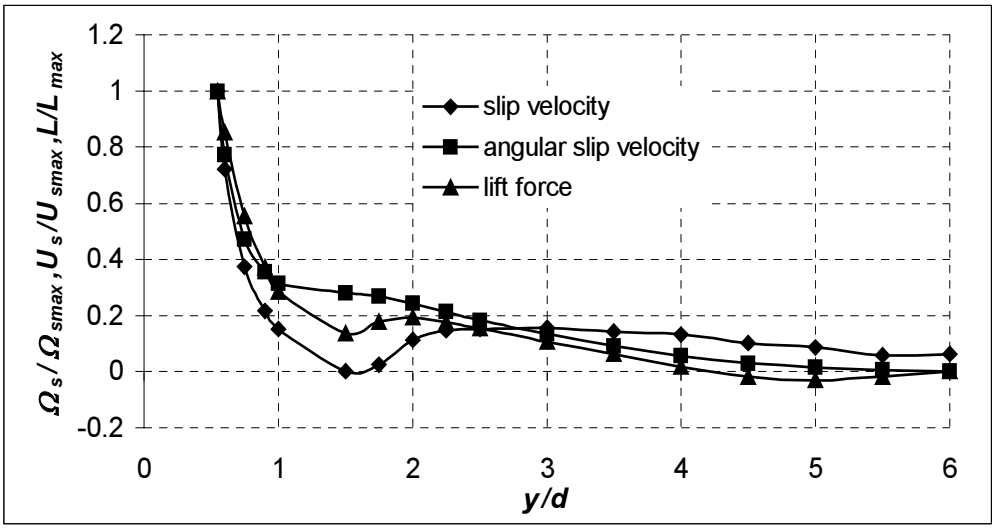

Figure B.7. The relative values of L, U_s and Ω_s in the steady flow with R=20 and n=0.9.

Dimensionless parameters based on local quantities are used to express the correlations. The local dimensionless net force is:

$$\lambda(y) = \frac{4\rho_f d\left[L(y) - (\rho_p - \rho_f)g\pi d^2/4\right]}{\pi\eta(y)^2} = \frac{4\rho_f d}{\pi\eta(y)^2} L_n(y)\,. \tag{B.10}$$

Two local Reynolds numbers are based on U_s and $\Omega_s - \Omega_{se}$ respectively:

$$R_U(y) = \frac{\rho_f U_s(y) d}{\eta(y)},\; R_\Omega(y) = \frac{\rho_f [\Omega_s(y) - \Omega_{se}] d^2}{\eta(y)}\,. \tag{B.11}$$

The product of R_U and R_Ω is defined as F:

$$F(y) = R_U \cdot R_\Omega = \frac{\rho_f^2 U_s(y)\left[\Omega_s(y) - \Omega_{se}\right] d^3}{\eta(y)^2}. \tag{B.12}$$

To compute $F(y)$ from (B.12), it is necessary to specify the equilibrium angular slip velocity $\Omega_{se}=\Omega_s(y_e)$ where y_e is the position at which the lift equals the buoyant weight. The $\hat{L}$ vs. y/d curve (Fig. B.3) shows that each and every value of y/d on the stable branches is a possible equilibrium position ($y=y_e$) for some particle ρ_p. You may cover the range of possible y_e by varying the weight of the particle. Once y_e is selected, Ω_{se} is given as $\Omega_s(y_e)$. The dependence of Ω_{se} and L_n on ρ_p makes the correlations between $\lambda(y)$ and $F(y)$ particle-density dependent. However, the steady state values of L do not depend

on particle density. If we derive the correlations between $\lambda(y)$ and $F(y)$ for one ρ_p, the lift force is essentially obtained and can be applied to particles with different densities. We present the correlations with the single equilibrium position of a neutrally buoyant particle as the reference. There are two advantages of this choice: the complexity of multi-equilibrium positions of a heavy particle is avoided; the correlations are in simple forms which are a power law for the stable branch near the wall and a linear relation for the stable branch near the centerline.

For a neutrally buoyant particle, a single equilibrium position exists at $y = y_e^N$ (the superscript is for "neutral") with $L(y_e^N) = 0$ and $\Omega_s(y_e^N) = \Omega_{se}^N$. Thus the dimensionless parameters have the following form:

$$\lambda(y) = \frac{4\rho_f dL(y)}{\pi\eta(y)^2} \text{ and } F(y) = \frac{\rho_f^2 U_s(y)\left[\Omega_s(y) - \Omega_{se}^N\right]d^3}{\eta(y)^2}.$$

The correlations are in the following form,

$\lambda(R,n,y/d) = a(R,n)F(R,n,y/d)^{m(R,n)}$ on the stable branch near the wall; (B.13)

$\lambda(R,n,y/d) = k(R,n)F(R,n,y/d)$ on the stable branch near the centerline. (B.14)

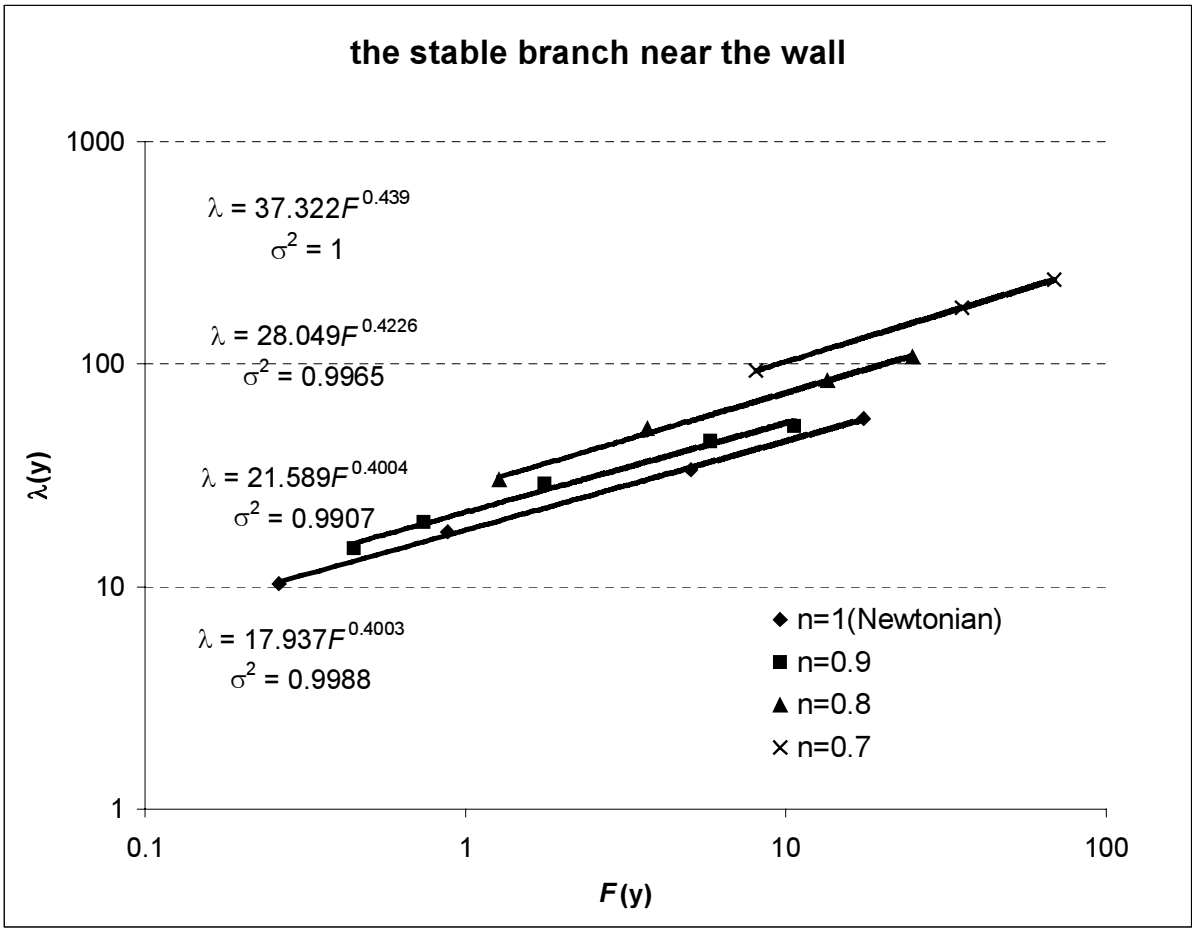

Figure B.8. The power law correlations between λ(y) and F(y) on the stable branch near the wall for the flows with R=20 and n=0.7, 0.8, 0.9 and 1 (Newtonian fluid).

We obtain the correlations for flows with n=0.7, 0.8, 0.9 and 1.0 (Newtonian fluid). In Fig. B.8, the correlations on the stable branch near the wall are plotted for the flows with R=20. The power law correlations along with the correlation coefficients σ^2 are shown in the figure. In Fig. B.9, two examples of the linear correlation between $\lambda(y)$ and $F(y)$ on the stable branch near the centerline are plotted for the flows with (R=20, n=0.7) and (R=80, n=0.8). It can be seen that our correlations describe the data faithfully.

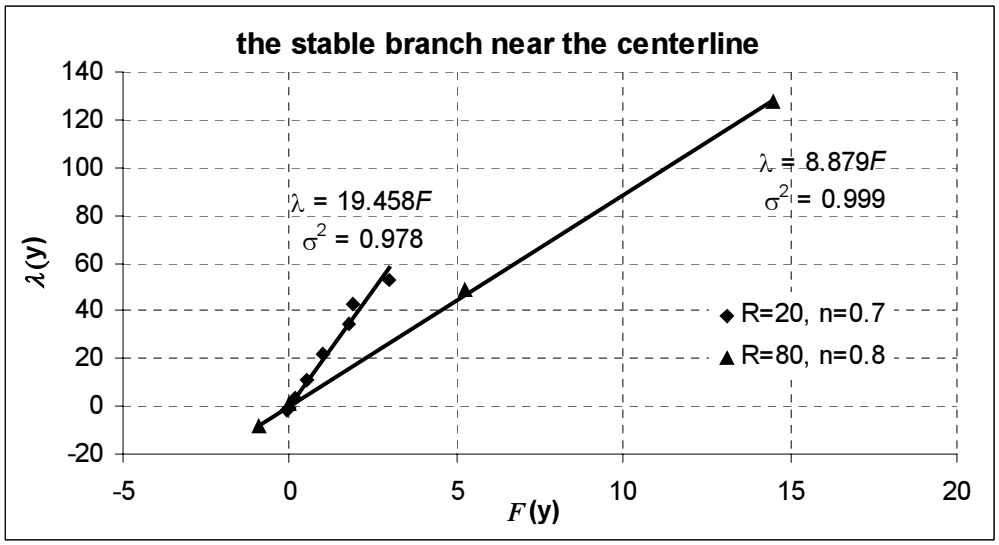

Figure B.9. The linear correlation between λ(y) and F(y) on the stable branch near the centerline for the flows with (R=20, n=0.7) and (R=80, n=0.8).

The prefactor a, the exponent m and the slope k in (B.13) and (B.14) are functions of R and n. In table B.4, the coefficients a, k and m are listed along with R, n, and the average Reynolds number $\overline{R}$ which can be viewed roughly as a parameter for the combined effects of R and n. Coefficients a, m and k are also plotted against $\overline{R}$ in Figs. B.10-B.12.

n	R	$\overline{R}$	a	m	k
1	20	20	17.937	0.4003	53.171
0.9	20	24.28	21.589	0.4004	34.685
0.8	20	30.48	28.049	0.423	27.348
0.7	20	39.7	37.322	0.439	19.458
1	40	40.0	27.288	0.410	30.739
0.9	40	51.84	36.38	0.427	25.591
0.8	40	69.97	40.808	0.481	22.166
0.7	40	97.89	9.664	0.774	11.759
1	80	80.0	38.009	0.448	24.35
0.9	80	110.72	53.729	0.450	21.066
0.8	80	160.06	9.570	0.779	8.879
0.7	80	237.6	2.710	0.898	7.698
1	120	120	43.83	0.472	21.54
1	160	160	41.48	0.496	16.39

Table B.4. The prefactor a, the exponent m and the slope k as functions of the shear index n and the Reynolds number R.

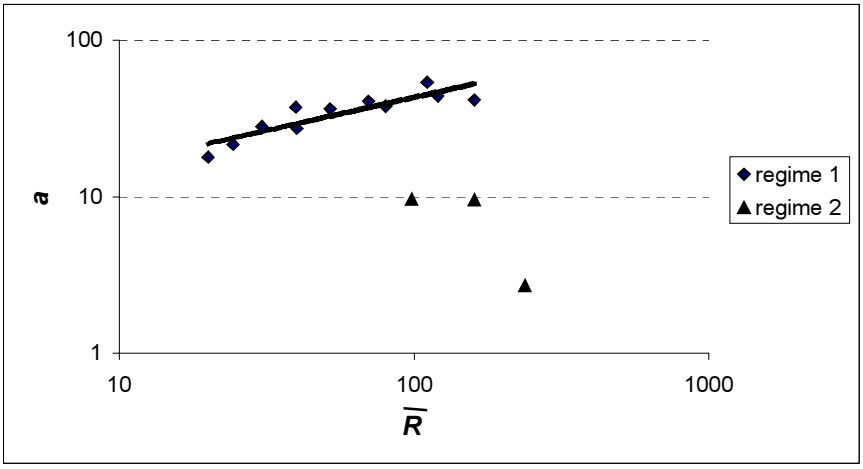

Figure B.10. The prefactor a vs. the average Reynolds number $\overline{R}$.

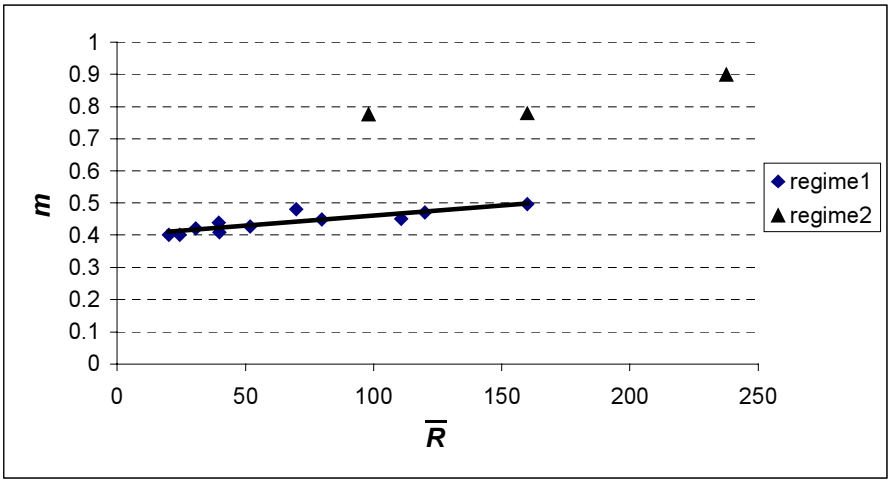

Figure B.11. The exponent m vs. the average Reynolds number $\overline{R}$.

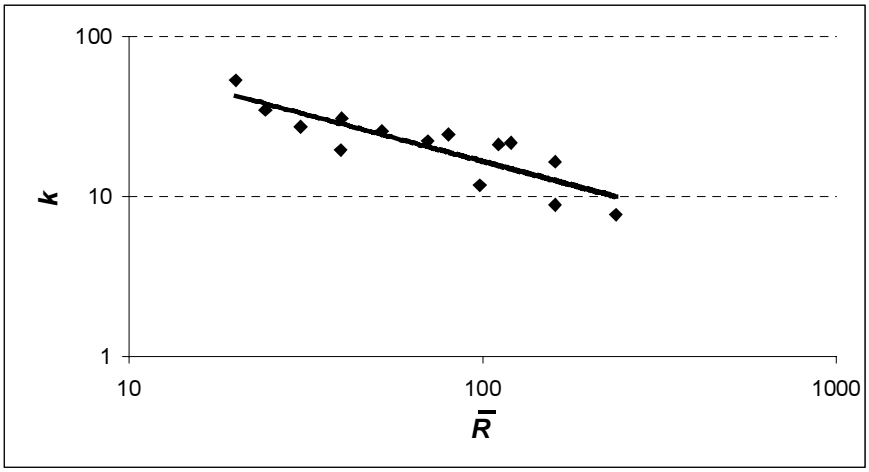

Figure B.12. The slope k vs. the average Reynolds number $\overline{R}$.

Figures B.10 and B.11 reveal that the power law correlation (B.13) on the stable branch near the wall has two regimes. Flows of Newtonian fluids and weak shear thinning flows fall into regime1 where the prefactor *a* increases with $\overline{R}$ increasing and the exponent *m* is in the range of 0.4 – 0.5. Regime2 has three flows (*n*=0.7, *R*=40), (*n*=0.7, *R*=80) and (*n*=0.8, *R*=80) and can be identified as a strong shear thinning regime where the prefactor *a* decreases with $\overline{R}$ increasing and the exponent *m* is in the range of 0.77 – 0.9. From the values of the exponent *m*, we can tell that in regime2 the dependence of the lift force on the product of slip velocities is stronger than that in regime1. It is noted that the two flows (*n*=1.0, *R*=160) and (*n*=0.8, *R*=80) have very close values of $\overline{R}$ but substantially different coefficients *a*, *m* and *k* (see table B.4); this indicates that particle lift in strong shear thinning flows is different with that in flows of Newtonian fluids at high Reynolds number. Figure B.12 exhibits one regime of the linear correlation (B.14) where the slope *k* decreases with $\overline{R}$ increasing. Figures B.10-B.12 also suggest that power law or linear functions of $\overline{R}$ could be used to approximate the prefactor *a* and the exponent *m* in regime1 and the slope *k*. However, the error of such approximations would be considerable. The reason of such error is that *a, k,* and *m* depend on both *n* and *R*; one single parameter $\overline{R}$ cannot fully describe the dependence of the coefficients on the flow.

We cannot fully determine the coefficients *a*, *m* and *k* as functions of *R* and *n* because of insufficient data. If we focus on flows of Newtonian fluids (*n*=1), *R* is the only active parameter and we expect to get satisfactory *a(R), k(R)* and *m(R)* approximations by data fitting analyses. The coefficients *a, k,* and *m* in flows of Newtonian fluids are listed as functions of *R* in table B.5.

R	*a*	*m*	*k*
20	17.94	0.400	53.17
40	27.29	0.410	30.74
80	38.01	0.448	24.35
120	43.83	0.472	21.54
160	41.48	0.496	16.39

Table B.5.The prefactor a, the exponent m and the slope k as functions of the Reynolds number R for flows of Newtonian fluids. Data are consistent with those in table B.4.

Data fitting analyses yield:

$$a = 5.34R^{0.428},\ \sigma^2=0.94; \tag{B.15}$$

$$m = 0.0007R + 0.386,\ \sigma^2=0.99; \tag{B.16}$$

$$k = 232.5R^{-0.515},\ \sigma^2=0.96. \tag{B.17}$$

Inserting (B.15), (B.16) and (B.17) into the correlations (B.13) and (B.14), we obtain correlations which apply to flows of Newtonian fluids with a Reynolds number in the range of 20 – 160.

$$\begin{cases} \lambda(y) = 5.34R^{0.428}F(y)^{(0.0007R+0.386)} & \text{on the stable branch near the wall;} \quad \text{(B.18)} \\ \lambda(y) = 232.5R^{-0.515}F(y) & \text{on the stable branch near the centerline.} \quad \text{(B.19)} \end{cases}$$

Replacing $\lambda(y)$ and $F(y)$ in (B.18) and (B.19) with their dimensional forms and re-arrange, we obtain the equations in the following form

$$\begin{cases} L = 4.20R^{0.428}\rho_f{}^{0.0014R-0.227}\eta_0{}^{-0.0014R+1.227}\left[U_s(\Omega_s-\Omega_{se}^N)\right]^{0.0007R+0.386}d^{0.0021R+0.159} \\ \qquad \text{on the stable branch near the wall;} \qquad \text{(B.20)} \\ L = 182.6R^{-0.515}\rho_f U_s(\Omega_s-\Omega_{se}^N)d^2 \\ \qquad \text{on the stable branch near the centerline.} \qquad \text{(B.21)} \end{cases}$$

Note that for Newtonian fluids, $\eta(y)$ reduces to η_0.

Although correlations (B.20) and (B.21) are derived using the equilibrium of a neutrally buoyant particle as the reference, they can be applied to heavy particles. To demonstrate this, we first obtain U_s and Ω_s for heavy particles at their equilibrium states from unconstrained simulations; these values are then inserted into (B.20) and (B.21) to calculate the lift forces which should match the values of the buoyant weight of the heavy particles. Two examples are shown in table B.6: a particle with ρ_p/ρ_f=1.016 in a flow with R =40 and a particle with ρ_p/ρ_f=1.045 in a flow with R =80. In both cases two stable equilibrium positions exist. The lift force for y_e close to the wall is computed using (B.20) and the lift force for y_e close to the centerline is computed using (B.21). It can be seen that the computed dimensionless lift forces are close to the values of the dimensionless buoyant weight (ρ_p/ρ_f-1) of the particles. In this way we demonstrate that the correlations derived for neutrally buoyant particles can be applied to heavy particles.

R	Ω_{se}^N (s^{-1})	ρ_p/ρ_f	ρ_p/ρ_f-1	y_e/d	Ω_s (s^{-1})	U_s (cm/s)	$\hat{L}$
40	0.2094	1.016	0.016	1.093	1.5765	0.2869	0.018
				2.377	1.1837	0.5393	0.014
80	0.4255	1.045	0.045	0.9476	4.332	0.4526	0.046
				2.705	2.737	0.8241	0.047

Table B.6. Computation of the lift forces on heavy particles using the correlations (B.20) and (B.21). The computed dimensionless lift forces are close to the values of the dimensionless buoyant weight (ρ_p/ρ_f–1) of the particles.

Correlations (B.20) and (B.21) apply to 2D motion of a particle in a Poiseuille flow. They may be compared to well-known lift expressions for a particle in a linear shear flow with shear rate $\dot{\gamma}$. The comparisons are at best tentative because the linear shear neglects the effects of the shear gradient which is a constant in the Poiseuille flow and not small; also because the lift expressions in linear shear flows are for indefinitely small Reynolds number perturbing Stokes flow on an unbounded domain. Bretherton [1962] found that the lift per unit length on a cylinder (2D sphere) at small values of $R = \dot{\gamma}a^2/\nu$ is given by

$$L = \frac{21.16\eta U_s}{(0.679 - \ln(\sqrt{R/4}))^2 + 0.634}. \qquad \text{(B.22)}$$

Saffman [1965] derived an expression for the lift on a sphere in a linear shear flow

$$L = 6.46\rho_f^{0.5}\eta^{0.5}U_s\dot{\gamma}^{0.5}a^2 + \text{lower order terms} \qquad \text{(B.23)}$$

where a is the radius of the sphere. The lower order terms are:

$$-U_s\, a^3 \rho_f \left[\pi \Omega_s - \left(\pi - \tfrac{22}{8}\right)\tfrac{1}{2}\dot{\gamma}\right]. \tag{B.24}$$

For a neutrally buoyant particle at equilibrium, $L = 0$ and from (B.22) and (B.23), $U_s = 0$. The Bretherton and Saffman formulas thus predict that the slip velocity is zero for a neutrally buoyant particle at equilibrium in an unbounded linear shear flow. Patankar *et al.* [2001] argued that zero slip velocity is always one solution for a neutrally buoyant particle freely moving in an unbounded linear shear flow, but it may not be the only solution and it can be unstable under certain conditions not yet understood. Feng, Hu and Joseph [1994] showed that a neutrally buoyant particle migrates to the centerline in a Couette flow where $U_s = 0$. From our simulations for 2D Poiseuille flows, $U_s \neq 0$ at the equilibrium position of a neutrally buoyant particle (see Fig. B.7); whereas $\Omega_s = \Omega_{se}$ at equilibrium gives rise to zero lift.

We find that our expression for the lift on the stable branch near the centerline (B.21) is similar to the leading term in Saffman's expression for the lift. If we make following changes in equation (B.21): $R = \dfrac{\rho_f V d}{\eta_0} \rightarrow R = \dfrac{\rho_f \dot{\gamma} d^2}{\eta}$, the power of R (-0.515) $\rightarrow$ (-0.5), and use $d = 2a$, equation (B.21) becomes:

$$L = 365.2 \rho_f^{0.5} \eta^{0.5} U_s \dot{\gamma}^{-0.5} (\Omega_s - \Omega_{se}^N) a \tag{B.25}$$

Comparing (B.25) and the leading term in (B.23), we note that both expressions are linear in U_s; both have a similar dependence on ρ_f, η, and a after noting that (B.25) is for the lift force per unit length. However, the dependence on $\dot{\gamma}$ and Ω_s-Ω_{se} is greatly different.

Another formula for the lift on a particle in an inviscid fluid in which uniform motion is perturbed by a weak shear was derived by Auton [1987] and a more recent satisfying derivation of the same result was given by Drew and Passman [1999]. They find that in a plane flow,

$$L = \frac{4}{3}\pi a^3 \rho U_s \Omega_f \tag{B.26}$$

where $\Omega_f = -\dot{\gamma}/2$. Expression (B.26) is similar to our correlation (B.21) but differs from (B.21) in several ways: (B.26) has a constant prefactor for inviscid fluids whereas viscous effects enter into (B.21) through R; the lift force depends on Ω_f - "spin" of the fluid in (B.26) but on the angular velocity discrepancy $\Omega_s - \Omega_{se}^N$ in (B.21); (B.26) is for 3D spheres and (B.21) is for 2D cylinders.

We compare the lift forces computed from the direct numerical simulation and from the lift expressions (B.21), (B.22), (B.23) and (B.26) in figure B.13. Our correlation (B.21) and Bretherton's expression (B.22) are for 2D cylinders and the dimensionless lift $\hat{L}$ is computed as $\hat{L} = L/(\rho_f g \pi d^2/4)$; Saffman and Auton's expressions (B.23) and (B.26) are for spheres and $\hat{L}$ is computed as $\hat{L} = L/(\rho_f g \tfrac{4}{3}\pi a^3)$. The slip velocity U_s, which is a functional of the solution, is prescribed in Bretherton, Saffman and Auton's expressions and undetermined in their theories. To calculate the lift forces from these expressions, we use the values of U_s obtained from our DNS. The values of U_s, Ω_s and

Ω_{se}^{N} obtained from the DNS are used in the calculation of (B.21).

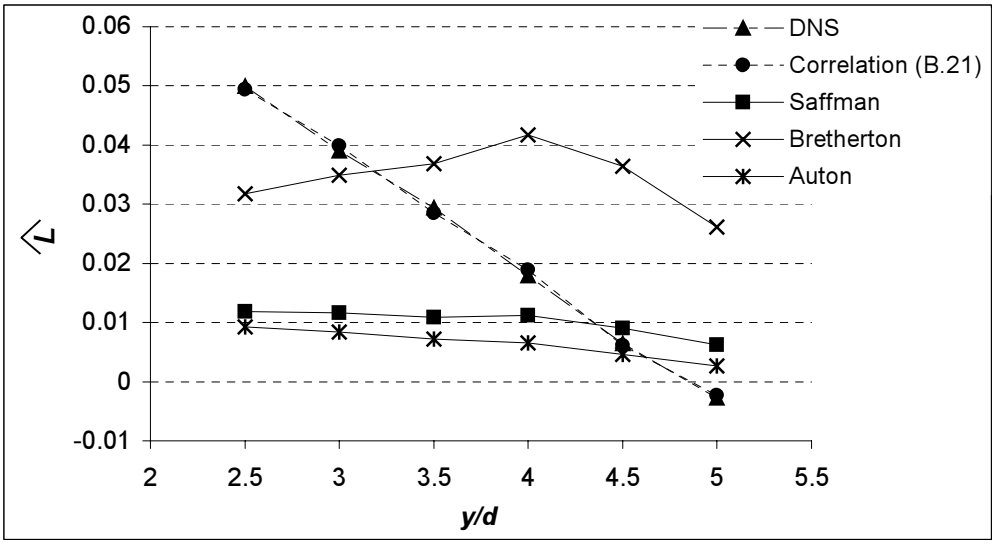

Figure B.13. A comparison of the lift forces computed from the direct numerical simulation and from the lift expressions (B.21), (B.22), (B.23) and (B.26). The lift forces on the stable branch near the centerline in a flow of Newtonian fluid with R=*80 are plotted.*

We draw the readers attention to the fact that the lift expressions (B.21), (B.22), (B.23) and (B.25) apply to different scenarios and are not strictly comparable. Our correlation (B.21) is for a freely rotating 2D cylinder without accelerations in a plane Poiseuille flow. Bretherton's expression (B.22) and Saffman's expression (B.23) are both for the lift on a particle in an unbounded linear shear flow with an indefinitely small Reynolds number; the difference is that the former applies to a non-rotating 2D cylinder while the latter applies to a rotating 3D sphere. Auton's expression (B.26) applies to a fixed 3D sphere in an inviscid fluid in which uniform motion is perturbed by a weak shear. Expressions (B.22), (B.23) and (B.26) cannot predict the change of sign across the equilibrium position; whereas our correlation (B.21) reproduces the DNS results faithfully.

Our correlations provide explicit expressions for the lift force on a particle in terms of the slip velocity U_s and the angular slip velocity discrepancy $\Omega_s - \Omega_{se}$. We emphasize that the relative angular motion is characterized by $\Omega_s - \Omega_{se}$ rather than Ω_s or Ω_f. By using the discrepancy, we are able to account for the Segrè and Silberberg effect. Our correlations cover the whole channel except the unstable regions. We believe that our correlations capture the essence of the mechanism of the lift force.

Correlations (B.20) and (B.21) are derived for L, U_s and Ω_s in steady flows, i.e., they apply to particles with zero acceleration. For a migrating particle, correlations (B.20) and (B.21) are not valid, although they might give good approximations when the acceleration of the particle is small. The application of such correlations is to determine parameters of a particle at equilibrium, e.g., the equilibrium position, translational velocity and angular velocity. For this end, correlations which relate U_s and Ω_s to prescribed parameters are needed. We will show derivation of such correlations is feasible in the next section.

- ***Correlations for slip velocity and angular slip velocity***

To make correlations (B.20) and (B.21) completely explicit, we need correlations which relate U_s and Ω_s to R and y/d in steady flows of Newtonian fluids. We illustrate the procedure for Ω_s. In Fig. B.14, the steady state values of $\Omega_s/(2\dot{\gamma}_w)$ obtained in constrained simulations are plotted against y/d for five values of R. If these data are plotted on a log-log plot of $\Omega_s/(2\dot{\gamma}_w)$ versus R, we obtain straight lines one for each value of y/d from the wall to the centerline (five of which are shown in Fig. B.15), leading to power law correlations:

$$\frac{\Omega_s(y/d,R)}{2\dot{\gamma}_w} = b(y/d)R^{r(y/d)} \;\Rightarrow\; \Omega_s(y/d,R) = b(y/d)R^{r(y/d)}\frac{R\eta_0}{\rho_f d^2}. \qquad \text{(B.27)}$$

The prefactor b and exponent r in these power law correlations, which are functions of y/d, are plotted in Fig. B.16. With more data points, these functions could be fitted to splines, making (B.27) completely explicit.

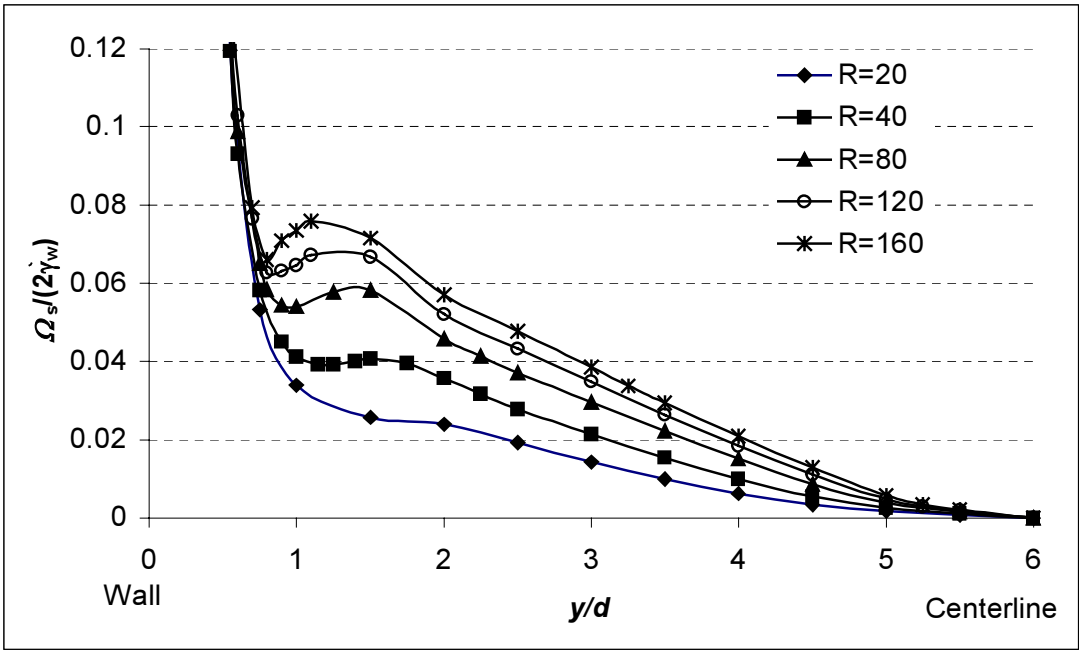

Figure B.14. The steady state values of the dimensionless angular slip velocity $\Omega_s/(2\dot{\gamma}_w)$ in flows of Newtonian fluids as a function of y/d.

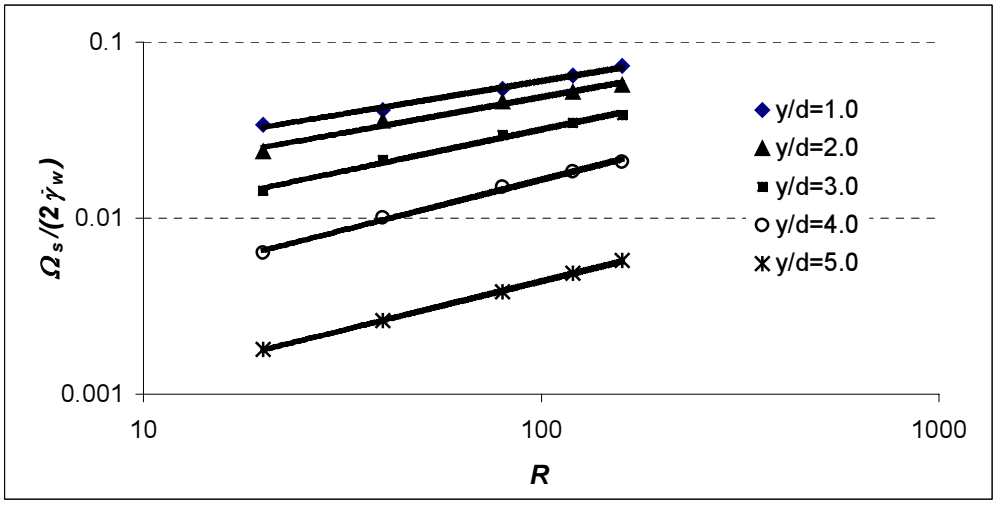

Figure B.15. Power law correlations between $\Omega_s/(2\dot{\gamma}_w)$ and R at five values of y/d.

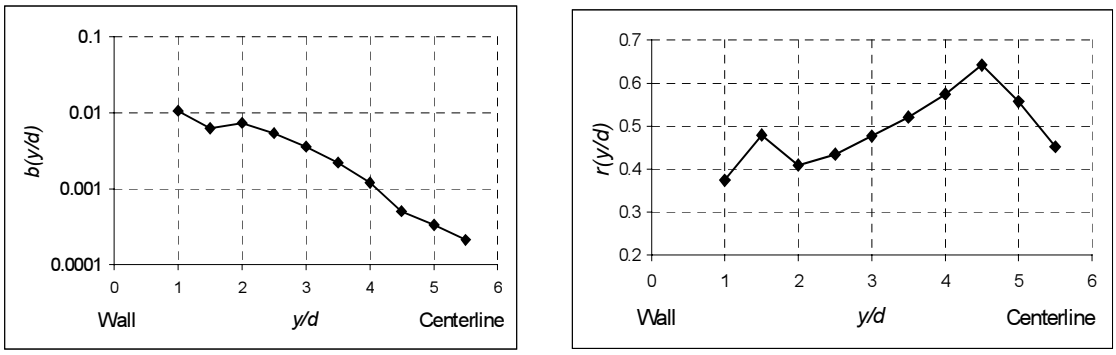

Figure B.16. The prefactor b and exponent r in correlation (B.27) as functions of y/d.

A similar procedure for U_s leads to

$$\frac{U_s(y/d,R)}{2\dot{\gamma}_w d} = c(y/d)R^{q(y/d)} \;\Rightarrow\; U_s(y/d,R) = c(y/d)R^{q(y/d)}\frac{R\eta_0}{\rho_f d}. \qquad \text{(B.28)}$$

As for *b* and *r* in (B.27), *c* and *q* could be fit to splines if more data points were available. Unlike correlation (B.27) which can be found at values of *y/d* from the wall to the centerline, correlation (B.28) can only be found at values of *y/d* on stable branches of steady solutions. It does not correlate well with the data for the unstable branches; in fact for some values of *R*, U_s is slightly negative at some values of *y/d* on the unstable branch near the wall, which is incompatible with a power law in the form (B.28).

In addition to (B.27) and (B.28), we also need a correlation between Ω_{se}^N, the angular slip velocity of a neutrally buoyant particle at equilibrium, and *R*, in order to make (B.20) and (B.21) completely explicit. Table B.7 shows that $\Omega_{se}^N/(2\dot{\gamma}_w)$ is essentially constant independent of *R*. Using the average of these values, we obtain:

$$\frac{\Omega_{se}^N(R)}{2\dot{\gamma}_w} = 5.21\times10^{-3} \;\Rightarrow\; \Omega_{se}^N(R) = 5.21\times10^{-3}\frac{R\eta_0}{\rho_f d^2}. \qquad \text{(B.29)}$$

R	20	40	80	120	160
$\Omega_{se}^N/(2\dot{\gamma}_w)$	5.06×10^{-3}	5.24×10^{-3}	5.32×10^{-3}	5.24×10^{-3}	5.21×10^{-3}

Table B.7. The dimensionless angular slip velocity of a neutrally buoyant particle at equilibrium is essentially a constant in flows of Newtonian fluids with R=20 – 160.

If we now insert (B.27) - (B.29) into (B.20) and (B.21), we obtain completely explicit (assuming sufficient data points for *b, r, c* and *q* to be fit to splines) correlations for the lift force:

$$\begin{cases} L = 4.20R^{0.0014R+1.2}\left\{c(\frac{y}{d})R^{q(\frac{y}{d})}[b(\frac{y}{d})R^{r(\frac{y}{d})}-5.21\times10^{-3}]\right\}^{0.0007R+0.386}\dfrac{\eta_0^2}{\rho_f d} \\ \qquad\qquad \text{on the stable branch near the wall;} \quad \text{(B.30)} \\ L = 182.6R^{1.485}c(\frac{y}{d})R^{q(\frac{y}{d})}[b(\frac{y}{d})R^{r(\frac{y}{d})}-5.21\times10^{-3}]\dfrac{\eta_0^2}{\rho_f d} \\ \qquad\qquad \text{on the stable branch near the centerline.} \quad \text{(B.31)} \end{cases}$$

These formulas allow us to calculate L for any value of y/d on the stable branches of the $\hat{L}$ vs. y/d curve (Fig. B.3), obviating the need for further numerical simulations.

The equilibrium position y_e/d of a particle of density ρ_p can be found as the value of y/d at which the lift force equals the buoyant weight:

$$L(y_e/d,R) = (\rho_p-\rho_f)g\frac{\pi d^2}{4};$$

the slip velocities at equilibrium can then be calculated by inserting y_e/d into (B.27) and (B.28):

$$\Omega_{se} = \Omega_s(y_e/d,R) = b(y_e/d)R^{r(y_e/d)}\frac{R\eta_0}{\rho_f d^2};$$

$$U_{se} = U_s(y_e/d,R) = c(y_e/d)R^{q(y_e/d)}\frac{R\eta_0}{\rho_f d}.$$

The corresponding translational velocity U_p and angular velocity Ω_p of the particle at equilibrium may then be calculated as $U_p = U_f(y_e) - U_{se}$ and $\Omega_p = \Omega_{se} - \dot{\gamma}(y_e)/2$.

▪ *Conclusions*

We study lifting of a cylindrical particle in plane Poiseuille flows of shear thinning fluids. It is known that certain regions in a channel are unstable and a particle cannot equilibrate in an unstable region. For example, Ho and Leal [1974] pointed out the centerline is an unstable equilibrium position in a 2D Poiseuille flow. Our studies show that the domain from the wall to the centerline in a 2D Poiseuille flow can be divided into four regions with the following order: wall – stable – unstable – stable – unstable – centerline. The distribution of these regions is affected by shear thinning. Our results indicate that when shear thinning effects become stronger, the unstable region at the centerline shrinks, indicating that the equilibrium position of a particle could be closer to the centerline.

The conclusion that the angular slip velocity discrepancy Ω_s - Ω_{se} changes sign across an equilibrium position established by Joseph and Ocando [2002] in Newtonian fluids is confirmed in shear thinning fluids. Across a stable equilibrium position, Ω_s - Ω_{se} has the same sign as the net lift force L_n; across an unstable equilibrium position, Ω_s - Ω_{se} has the opposite sign as the net lift force L_n.

Correlations for the lift force on a particle in terms of the slip velocity U_s and the angular slip velocity discrepancy Ω_s - Ω_{se} are derived. The correlations are a power law near the wall and a linear relation (which can be taken as a power law with the power of one) near the centerline. The correlations apply to both neutrally buoyant and heavy particles and cover the whole channel except the unstable regions. Two regimes, one with no or weak shear thinning effects and the other with strong shear thinning effects, are identified for the power law correlation (B.13) whereas only one regime is found for the linear correlation (B.14). It is noted that particle lift in strong shear thinning flows is different with that in flows of Newtonian fluids at high Reynolds number.

We are able to obtain correlations between L and $U_s(\Omega_s - \Omega_{se})$ with coefficients expressed as functions of R; these correlations cover the flows of Newtonian fluids with the Reynolds number in the range of 20 - 160. The correlation is compared to well known analytical expressions for lift force in shear flows and similarities between them are revealed. The major difference between them is that the angular slip velocity discrepancy Ω_s - Ω_{se} is used in our correlations instead of the shear rate or Ω_s. We also demonstrate that correlations which relate U_s and Ω_s to prescribed parameters can be constructed and will make the correlations for L completely explicit. Thus the lift force in steady flows can be calculated using correlations at any value of y/d on stable branches from the prescribed parameters; the equilibrium position of a particle with a certain density can then be determined by the balance between the lift force and its buoyant weight.